Available online at www.eccomasproceedia.org
Eccomas Proceedia COMPDYN (2023) 3856-3868

ECCOMAS
Proceedia

COMPDYN 2023
9th ECCOMAS Thematic Conference on
Computational Methods in Structural Dynamics and Earthquake Engineering
M. Papadrakakis, M. Fragiadakis (eds.)
Athens, Greece, 12-14 June 2023

A 3D FRACTURE ENERGY-BASED SMEARED CRACK APPROACH FOR THE NONLINEAR BEHAVIOR OF REINFORCED CONCRETE STRUCTURES.

Christos Mourlas[1], George Markou[2] and Manolis Papadrakakis[3]

[1] Czech Technical University in Prague, Faculty of Civil Engineering, Thákurova 7, 166 29 Prague,Czech Republic
christos.mourlas@fsv.cvut.cz

[2] Department of Civil Engineering, University of Pretoria, South Africa
e-mail: george.markou@up.ac.za

[3] Department of Civil Engineering, National Technical University of Athens, Greece
e-mail: mpapadra@central.ntua.gr

Abstract

This research study presents a novel energy-based constitutive model of concrete in the framework of the smeared crack approach. The proposed model constitutes an extension to a previous numerical model [1,2] with an addition of a fracture energy-based algorithmic approach developed by [3]. The uncracked behavior of concrete is based on the experimental evidence of the triaxial behavior of concrete described in the literature [4]. The cracked behavior of concrete is modelled with a fracturing approach while cracking is treated with the smeared crack approach. The proposed modelling approach manages to capture the behavior of reinforced concrete (RC) structures with computational efficiency and numerical accuracy as it combines the experimental triaxial behavior of concrete in an algorithmic framework that can alleviate numerical issues of nonlinear concrete behavior such as cracking. The numerical simulation is implemented by using hexahedral isoparametric finite elements for discretizing the concrete domain and truss elements for the steel reinforcement. The proposed approach has been tested on two RC specimens focusing on structural members with insufficient shear reinforcement and high shear stresses. The numerical behavior has been validated by the comparison of the numerical with experimental data found in the international literature. The effect of choosing different approaches of the smeared crack method (fixed and rotated) is also investigated.

Keywords: Cracking, Fracture, smeared crack approach, 3D FEM, Detailed modeling, Shear behavior.

ISSN:2623-3347
Peer-review under responsibility of the organizing committee of COMPDYN 2023.
doi: 10.7712/120123.10685.21078

1 INTRODUCTION

In the last few decades, many numerical models have been proposed to simulate the mechanical behavior of reinforced concrete (RC) structures. Many models can be found in the literature that can describe specific aspects of concrete behavior and their applications are limited to certain cases of little practical interest. These constitutive models emphasize the post-peak material by introducing several material parameters. The values of these parameters are usually calculated after a parametric investigation in an attempt to directly match the numerical and experimental results by reverse-engineering the problem. This approach leads to the loss of objectivity and the inability to use this approach to perform predictive analysis.

The constitutive model of the behavior of concrete must describe a realistic behavior of concrete under a generalized three-dimensional state of stress. The key features of every numerical approach must consider:

1. Nonlinear stress-strain behavior under a multiaxial state of stress.
2. Strain softening behavior and the anisotropic elastic degradation.
3. Progressive cracking caused by tensile stress and strains.

There are many models proposed for RC structures, in the literature [1-6]. Each model has its advantages and disadvantages resulting from its limitations. Many models combine plasticity formulations for concrete behavior under compression with fracture energy-based approaches for tension [3]. In addition, several models based on damage mechanics [7, 8] are proposed for the behavior of concrete under monotonic and cyclic loading conditions.

However, a numerical approach combined with a constitutive model for concrete behaviour that produces accurate and computationally efficient results for any RC structural member is still an open research topic. An accurate, objective, and computationally efficient approach will be a powerful tool for any professional civil engineer and scientist studying the seismic behavior of existing RC structures or performing the design of retrofit interventions for severely deteriorated RC structures.

The model proposed in [1], describes the triaxial behavior of concrete without the need of introducing numerous parameters of the concrete material. The proposed constitutive relations have been derived from the experimental and numerical work of Kotsovos and Pavlovic [4]. The only parameters required to be defined in their proposed algorithmic approach [4], are the uniaxial compressive strength, the tensile strength, Young's modulus, and Poisson's ratio. The model has been improved in [2] where damage factors have been introduced that they are being automatically defined according to the number of cycling loads and the number of cracks. The key features of this numerical approach are accuracy, numerical simplicity and stability, and computational efficiency. These features made the model attractive even for the analysis of large-scale structures [9].

The accuracy of the model is mainly based on the smeared crack approach and the algorithmic approach that has been applied for every stress state [2]. However, this approach can lead to excessive cracking in order to represent a severely damaged state. Although the model doesn't appear to have mesh sensitivity issues [10], it is difficult to prove with the current algorithmic approach. To control the smeared cracking, a crack band approach [11] must be applied.

In this article, a connection between two algorithmic approaches is proposed and tested in terms of computational stability and numerical accuracy. In addition, a discussion takes place in relation to the use of different smeared crack approaches and how every approach affects the behavior of the RC numerical model. Finally, the model is examined and its ability to model RC structures that are subjected to monotonic loading conditions is evaluated.

2 UNCRACKED CONCRETE MATERIAL CONSTITUTIVE MODEL

The stress-strain relationships are expressed by decomposing each state of strain and stress into hydrostatic and deviatoric components. Therefore, the normal and shear octahedral stresses (σ_0, τ_0) and strains (ε_0, γ_0) are used. It is known that hydrostatic stresses σ_0 induce the variation of the volumetric strain $\varepsilon_{0(h)}$, while the application of deviatoric stresses τ_0 cause both volumetric and deviatoric strains. The combined approach presented by Kotsovos and Pavlovic [4] is based on the use of the bulk modulus *K* and the shear modulus *G* which describe the non-linear σ_0-$\varepsilon_{0(h)}$ and τ_0-$\gamma_{0(d)}$ behavior combined with the use of σ_{id} to take into account the coupling effect of τ_0-$\varepsilon_{0(d)}$ (*h* and *d* stand for hydrostatic and deviatoric components, respectively). The σ_{id} is an equivalent external stress which can be added to the externally applied hydrostatic stress. The constitutive relations take the following form:

$$\varepsilon_0 = \varepsilon_{0(h)} + \varepsilon_{0(d)} = (\sigma_0 + \sigma_{id}) / (3K_s) \tag{1}$$

$$\gamma_0 = \gamma_{0(d)} = \tau_0 / (2G_s) \tag{2}$$

where K_s and G_s are the secant forms of bulk and shear moduli, respectively. An extensive experimental investigation in [4] led to the analytical expressions of the σ_{id} and the secant and tangent forms of bulk and shear modulus as functions of the current state of stress (σ_0, τ_0, f_c). The analytical expressions obtained by regression analysis, have this form:

$$K_s / K_e = 1/[1 + A(\sigma_0 / f_c)^{b-1}] \quad \text{for } \sigma_0 / f_c \le 2 \tag{3a}$$

$$K_s / K_e = 1/[1 + 2^{b-1} Ab - 2^b (b-1) A(\sigma_0 / f_c)^{-1}] \text{ for } \sigma_0 / f_c > 2 \tag{3b}$$

$$G_s / G_e = 1/[1 + C(\tau_0 / f_c)^{d-1}] \tag{4}$$

$$\sigma_{id} / f_c = M(\tau_0 / f_c)^n \tag{5}$$

where the parameters *A, b, C, d, M,* and *n* are calculated by the expressions (as a function of the uniaxial compressive strength f_c) in Table 1.

$A = 0.516$ for $f_c \le 31.7$ $A = 0.516/[1 + 0.0027(f_c - 31.7)^{2.397}]$ for $f_c > 31.7$	$M = k/[1 + l(\sigma_0 / f_c)^m]$
	$k = 4/[1 + 1.087(f_c - 15)^{0.23}]$
$d = 2.12 + 0.0183 f_c$ for $f_c \le 31.7$ $d = 2.7$ for $f_c > 31.7$	$l = 0.222 + 0.01086 f_c - 0.000122 f_c^2$
	$m = -2.415$ for $f_c \le 31.7$ $m = -3.531 + 0.0352 f_c$ for $f_c > 31.7$
$C = 3.573$ for $f_c \le 31.7$ $C = 3.573/[1 + 0.0134(f_c - 31.7)^{1.414}]$ for $f_c > 31.7$	$n = 1$ for $f_c > 31.7$ $n = 0.3124 + 0.0217 f_c$ for $f_c > 31.7$

Table 1 Expression of parameters *A, b, C, d, M*, and *n* as functions of f_c that are used in the concrete material model.

The strains expressed in the global coordinate system are determined by the use of the expression in Eq. 1 and take the following equivalent form:

$$\varepsilon_{ij} = (\sigma_{ij} + \sigma_{id}\delta_{ij}) / (2G_s) - (3\nu_s / E_s)(\sigma_0 + \sigma_{id})\delta_{ij} \tag{6}$$

where E_s (σ_o, τ_o, f_c) and ν_s (σ_o, τ_o, f_c) are the secant Young's modulus and Poisson's ratio, respectively, and are derived from K_s and G_s by the following standard formula of linear elasticity:

$$E_s = (9K_sG_s) / (3K_s + G_s),\ \nu_s = (3K_s - 2G_s) / (6K_s + 2G_s) \tag{7}$$

During the nonlinear procedure, the stress and strain increments are calculated using the tangent expressions K_t, G_t, E_t, and ν_t as presented in [4]. The expression of Eq. 6 is used in order to correct the stresses and strains taking into account stress σ_{id} which represents the coupling effect between τ_0 and $\varepsilon_{0(d)}$. The constitutive matrix of the proposed 3D material model can take the following form:

$$D = \begin{bmatrix} 2G_t + \mu & \mu & \mu & 0 & 0 & 0 \\ \mu & 2G_t + \mu & \mu & 0 & 0 & 0 \\ \mu & \mu & 2G_t + \mu & 0 & 0 & 0 \\ 0 & 0 & 0 & G_t & 0 & 0 \\ 0 & 0 & 0 & 0 & G_t & 0 \\ 0 & 0 & 0 & 0 & 0 & G_t \end{bmatrix} \tag{8}$$

where $\mu = K_t - 2G_t/3$ and $K_t = K_t(\sigma_0, \tau_0, f_c)$, $G_t = G_t(\sigma_0, \tau_0, f_c)$. It is assumed that the uncracked concrete behaves elastically at low-stress levels. Particularly, when the deviatoric stress of an uncracked Gauss Point (GP) of a concrete element, is less than 50% of the corresponding ultimate strength, then the elastic constitutive matrix is used [1]. Otherwise, the constitutive material matrix is updated using the tangent expressions of bulk and shear moduli.

3 CRITERION OF FAILURE

The value of ultimate deviatoric stress may be interpolated by the τ_{0e} and τ_{0c} stresses using the expressions of Willam and Warnke [12].

$$\begin{aligned} \tau_{0u} = \{&2\tau_{0c}(\tau_{0c}^2 - \tau_{0e}^2)\cos\theta + \tau_{0c}(2\tau_{0e} - \tau_{0c}) \\ &[4(\tau_{0c}^2 - \tau_{0e}^2)\cos^2\theta + 5\tau_{0e}^2 - 4\tau_{0c}^2\tau_{0e}^2]^{1/2}\} / [4(\tau_{0c}^2 - \tau_{0e}^2)\cos^2\theta + (2\tau_{0e} - \tau_{0c})^2] \end{aligned} \tag{9}$$

The τ_{0e} (θ=0°) corresponds to the state of $\sigma_1 = \sigma_2 > \sigma_3$ (triaxial extension), while τ_{0c} (θ = 60°) correspond to the state of $\sigma_1 > \sigma_2 = \sigma_3$ (triaxial compression). It is also known that concrete's strength under tension is unaffected by triaxial phenomena. Therefore, it is considered that concrete fails in tension when a tensile stress σ_{ij} exceeds the tensile strength of concrete f_{ct}. The schematic representation of the ultimate strength is shown in Fig. 1.

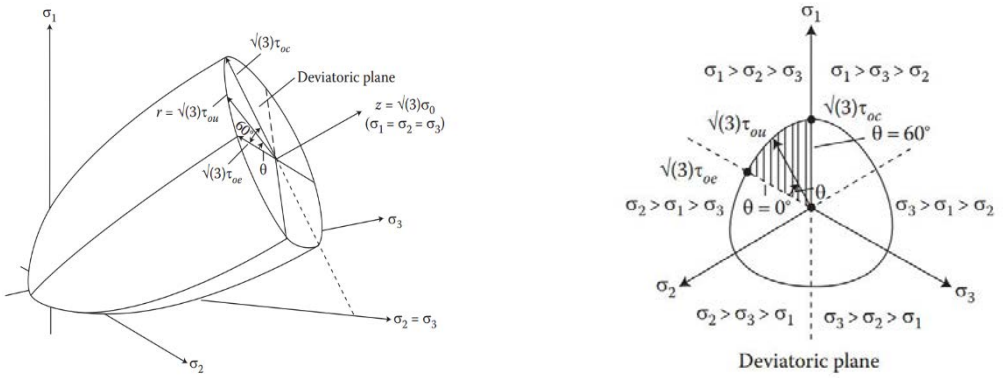

Figure 1 Schematic representation of the ultimate-strength surface : (a) general view in stress space, (b) typical cross-section of the strength envelope with a deviatoric plane (a plane of constant σ0, viewed along the axis $\sigma_1 = \sigma_2 = \sigma_3$).[4]

The expressions of τ_{0e} and τ_{0c} are derived by an experimental investigation as shown here:

$$\tau_{0c} / f_c = 0.944(\sigma_0 / f_c + 0.05)^{0.724} \tag{10}$$

$$\tau_{0e} / f_c = 0.633(\sigma_0 / f_c + 0.05)^{0.857} \tag{11}$$

4 FRACTURE MODELLING

The fracture modelling approach proposed by Cervenka et al. [3] is used in this work. When the criterion of failure is satisfied, then the fracture model is activated. The model assumes small strains and it can be written as:

$$\varepsilon_{ij} = \varepsilon_{ij}^{e} + \varepsilon_{ij}^{f} \tag{12}$$

Therefore, the stress development that shows the material degradation can be described by the following rate equations:

$$\sigma_{ij} = D_{ijkl} \cdot \left(\varepsilon_{kl} - \varepsilon_{kl}^{f} \right) \tag{13}$$

Also, the evolution of the fracture rate ε_{kl}^{f} is governed by the following flow rule:

$$\varepsilon_{kl}^{f} = \lambda^{f} \cdot m_{ij}^{p}, m_{ij}^{p} = \frac{\partial g^{f}}{\partial \sigma_{ij}} \tag{14}$$

where λ^{f} is the inelastic fracturing multiplier, and g^{f} is the potential defining the direction of inelastic fracturing strains in the fracturing model.

It is considered that, when the criterion of failure is satisfied and the specimen is under tension, one of the principal stresses exceeds the tensile strength. Therefore, in tension, the failure surface is transformed into a Rankine failure surface. The principal stress (along the principal direction p) in the case of cracking under tension must satisfy the following equation:

$$f_p^{f} = {}^{t}\sigma_{ij}\, n_i^{p}\, n_j^{p} - D_{ijmn}\, d\varepsilon_{mn}^{f}\, n_i^{k}\, n_j^{k} - f_t = 0 \tag{15}$$

where ${}^{t}\sigma_{ij}$ is a trial elastic prediction that has been made taking into account the current stain state. Assuming an associated form (g^f=f^f) for the fracturing strain increment, Eq. 14 takes the following form:

$$d\varepsilon_{ij}^{fp} = d\lambda^p \cdot \frac{\partial f_p^f}{\partial \sigma_{ij}} = d\lambda^p \cdot n_i^p \cdot n_j^p \tag{16}$$

After substituting Eq. 16 into Eq. 15, the fracturing multiplier can be expressed in the following form:

$$d\lambda^p = \frac{{}^{t}\sigma_{ij}\, n_i^p\, n_j^p - f_t(w^p)}{D_{ijmn}\, n_i^p\, n_j^p\, n_m^p\, n_n^p} \tag{17}$$

where,

$$w^p = L_t\left(\hat{\varepsilon}_p + d\lambda^p\right) \tag{18}$$

Eqs. 17 and 18 must be solved iteratively since for softening materials the tensile strength is a function of crack opening w^p. The crack opening is defined by the following expression suggested by Hordijk [13]:

$$\frac{\sigma}{f_t} = \left[1 + \left(c_1 \frac{w}{w_0}\right)^3\right] e^{-c_2 \frac{w}{w_0}} - \frac{w}{w_0}(1 + c_1^3) e^{-c_2} \tag{19}$$

where σ is the tensile concrete stress normal to crack, f_t is the concrete tensile strength, $c_1 = 3$, $c_2 = 6.93$, $w_0 = 5.14\, G_f / f_t$, and G_f is the fracture energy of the material. In Eq. 18, the L_t represents the characteristic length used as a crack band size introduced by Bazant and Oh (1983). The suggested limits for the values of the characteristic length related to the size of the finite elements from the work of Cervenka et al. [3], have been adopted for the needs of this work.

The local fracturing strains can be calculated by using the expression of Rots and Blaauwendraad [14]:

$$\varepsilon^f = (D + D^{cr})^{-1} D\, \varepsilon \tag{20}$$

where D_{cr} is the stiffness inside the crack zone. It is defined by the following formulas:

- Mode I

$$D_{pppp}^{cr} = \frac{f_t(w^p)}{\hat{\varepsilon}_p^f} \tag{21}$$

- Mode II and III

$$D_{ijij}^{cr} = min\left(D_{iiii}^{cr}, D_{jjjj}^{cr}\right) \cdot r^g \tag{22}$$

where r^g is the shear coefficient which is an input parameter of the model. For the above expressions, large penalty numbers $D_{pppp}^{cr} = \frac{f_t(0)}{e}$ (where e is a small number) are used to avoid cases during the onset of cracking that they may lead the above expression to infinity. The secant constitutive matrix in the material directions can be derived from Eq. 13 using Eq. 20:

$$D_s = D - D \cdot \left(D^{cr} + D\right)^{-1} \cdot D \tag{23}$$

The model is further described by Cervenka et al., [3]. The flow chart that describes the algorithm through which the model has been applied for a single GP is shown in Fig. 2.

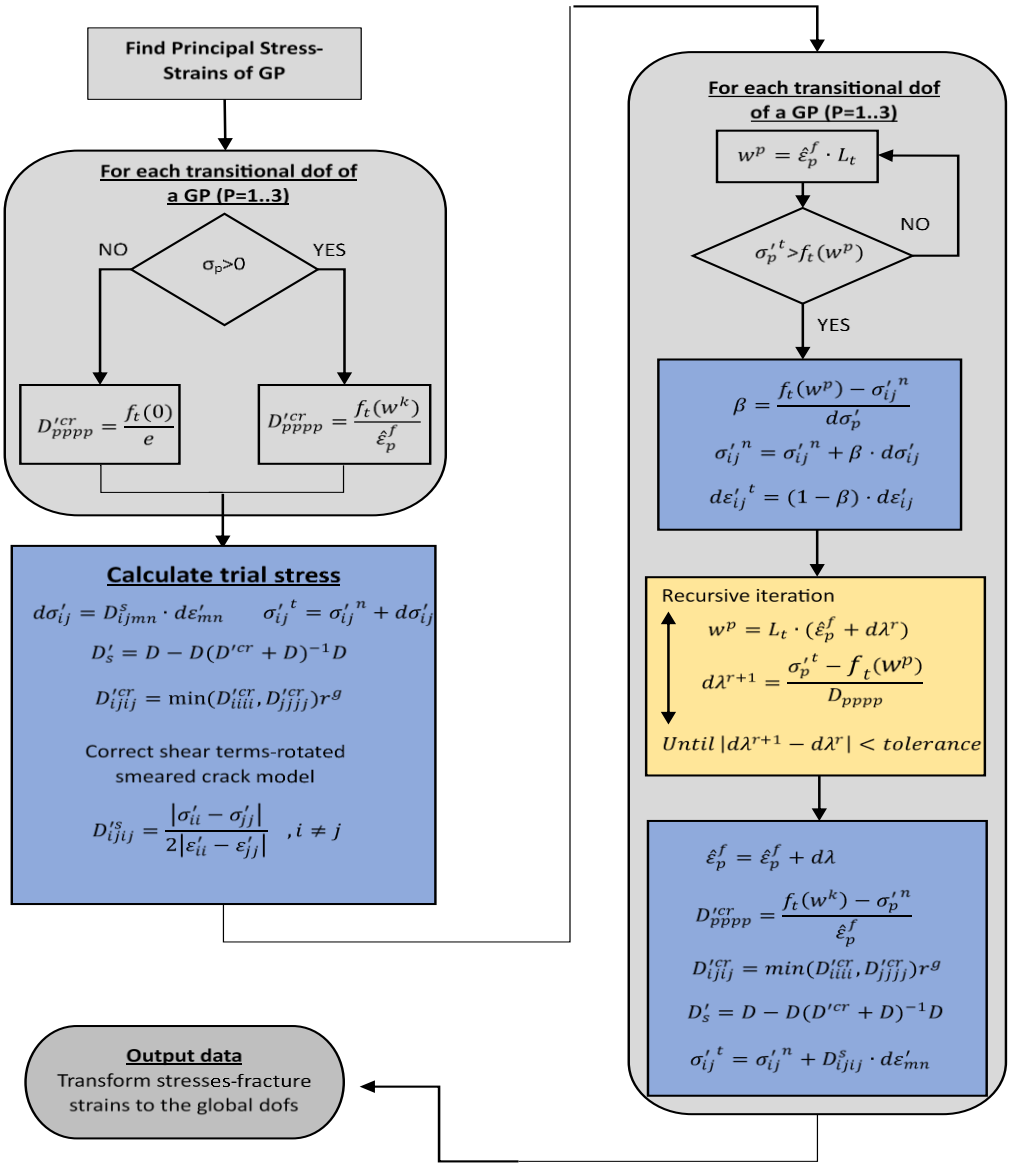

Figure 2 Flow chart of the fracture model of concrete (adapted from [3])

According to the above-described formulations of concrete behaviour of concrete under tension [3] and compression [4], the proposed concrete material model combines the two different theories in an attempt to derive a more accurate material model. This is evaluated through the use of experimental data that are used to assess the ability of the proposed material model in capturing the behaviour of RC specimens that develop significant shear deformation. The following section discusses a first set of numerically obtained results.

5 NUMERICAL APPLICATIONS

5.1 Leonhart's shear beam

The well-known Leonhart's shear beam (Leonhardt and Walther [15]) is examined to validate the proposed constitutive approach using three-dimensional hexahedral isoparametric finite elements, where the steel reinforcement is modeled through the use of embedded truss elements. The shear beam does not have shear reinforcement (stirrups) and according to the experimental data [15], it develops a severe shear failure at the end of the test. The geometry of the RC specimen which was tested through a four-point bending test, is presented in Fig. 3. Due to symmetry, half of the beam is modelled herein using the appropriate boundary conditions, which also allows its modeling through ATENA software. It must be also noted here that for the case of the proposed material model, the analysis foresees a displacement control nonlinear analysis.

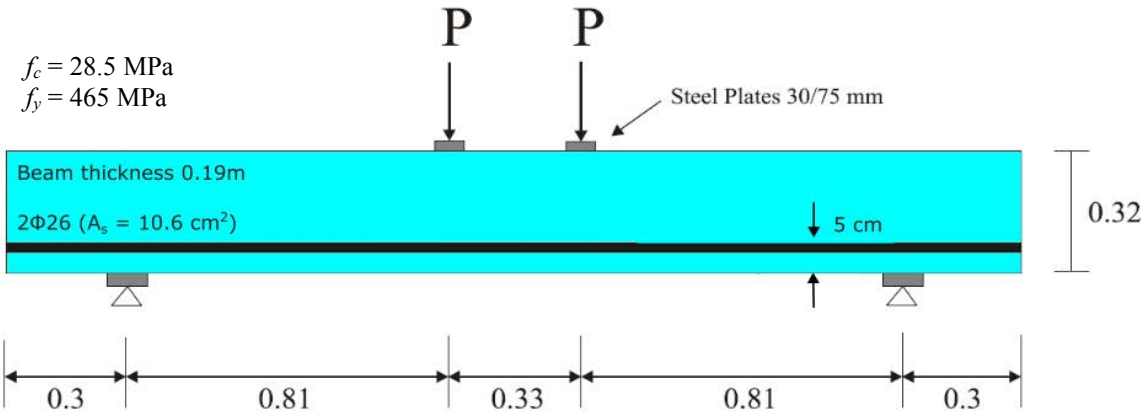

Figure 3 Leonhart's shear beam. Geometric and reinforcement details (adapted from [3]).

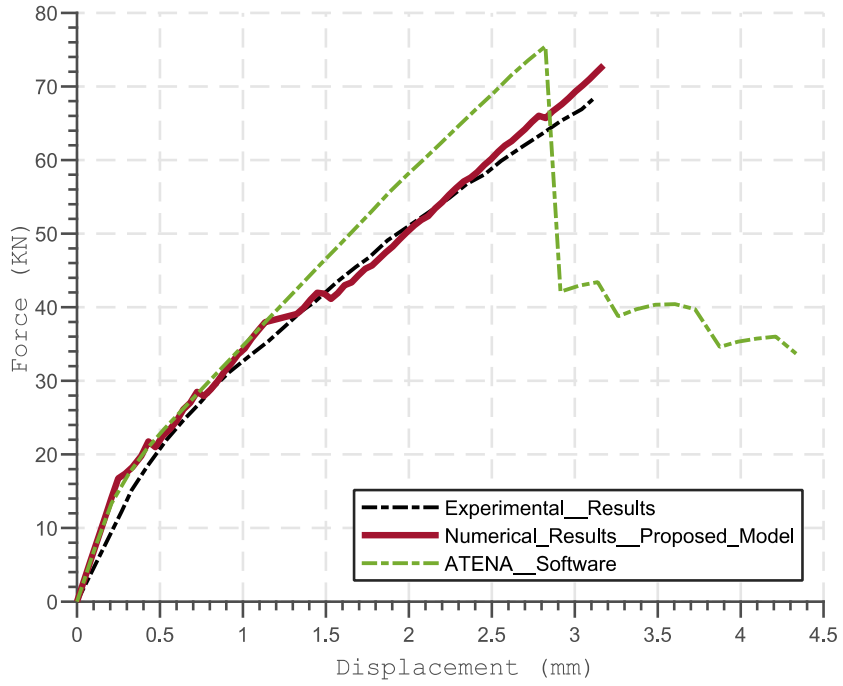

Figure 4 Leonhart's shear beam. Comparison of the numerical results with the experimental data.

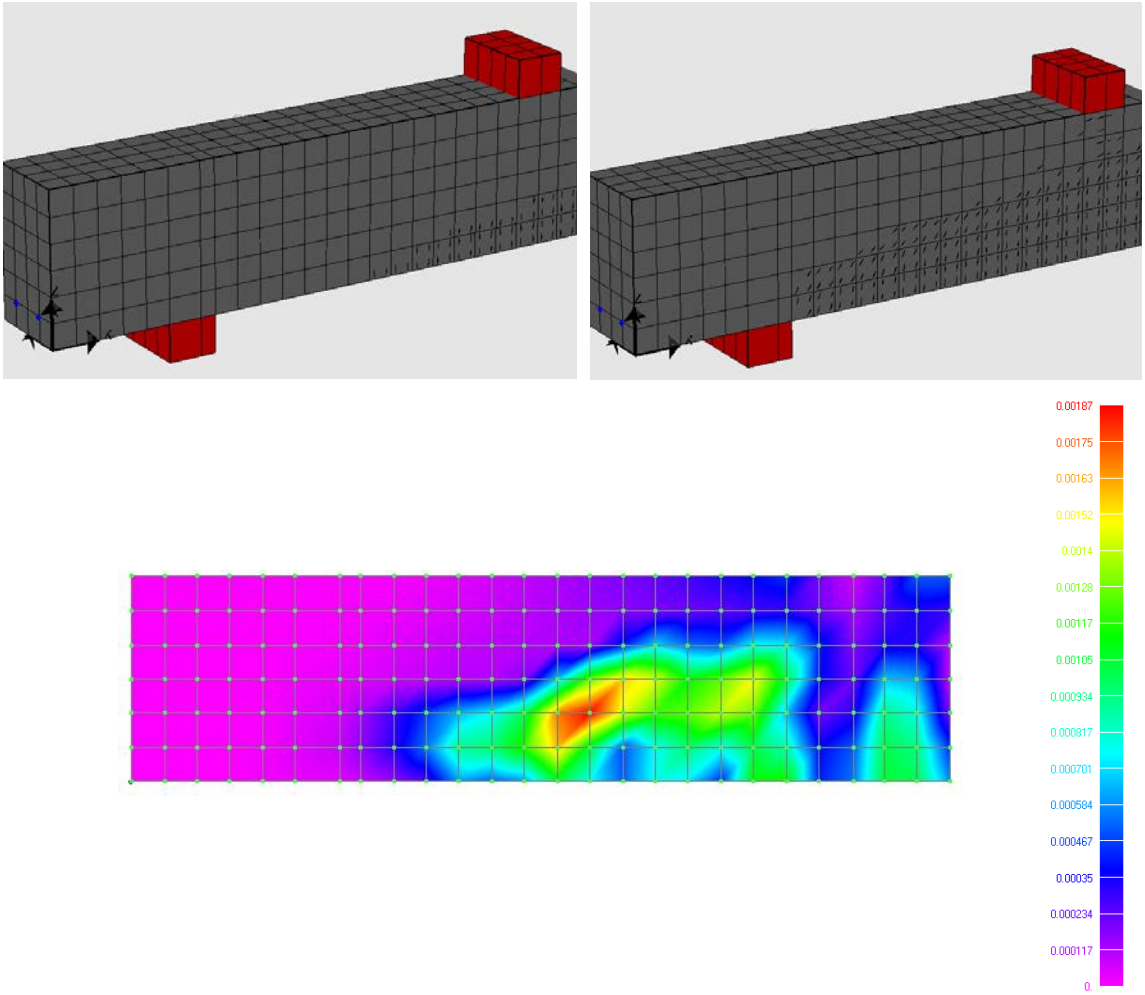

Figure 5 Crack pattern (Left) at first crack opening and (Right) prior to failure. (Down) Solid von Mises strain contour prior to failure.

As it was stated above, the concrete domain is modelled by 8-noded hexahedral finite elements, and the steel reinforcement is modelled by truss finite elements. The numerical results are compared with the experimental ones in Fig. 4. Additionally, the numerical results are compared with the numerical results obtained by ATENA software [16]. According to the curves in Fig. 4, it is easy to observe that the proposed constitutive model derives the best results when compared to the curve obtained by ATENA software that uses the model for both tension and compression of concrete as it was presented in [3]. It is also very interesting to note that the proposed material model manages to capture the concrete material deterioration in an almost perfect manner as the experiment evolves, while the model that adopts the material model proposed in [3] fails to do so. It is noteworthy to state here that ATENA was also used herein to perform a displacement control analysis. It is evident and undeniable that the overall RC response that derives from the ATENA software [16] that uses the Cervenka et al., [3] material model is not realistic in this regard since it fails to capture the basic mechanical response that RC structures usually exhibit, especially when the reinforcement ratio is low.

The crack patterns in Fig. 5 show that the crack development starts from small diffused flexural cracks near the midspan which eventually lead to a large shear crack between the point of the applied load and the support (see the crack pattern and solid von Mises contour in Fig. 5). This is in line with the crack formation reported in [15].

5.2 Lefas and Kotsovos shear wall

The RC shear wall specimen which is investigated experimentally in Lefas and Kotsovos [17], is denoted as shear wall SW31 and numerically studied herein. The geometric details of the RC shear wall are illustrated in Fig. 6, where it can be seen that is 650 mm wide, 1300 mm height, and 70 mm thick. The uniaxial compressive strength (f_c) of SW31 was 35.2 MPa which is also the value defined within the proposed material model. The yielding stresses (f_y) of the steel reinforcement were 420, 520, and 470 MPa for the 4-, 6- and 8-mm diameter bars used, respectively. The shear wall was subjected to different cyclic loading conditions.

The concrete domain is modelled by 8-noded hexahedral finite elements, and the steel reinforcement is modelled with embedded truss finite elements. At the top and the bottom of the shear wall, 81 rigid 8-noded hexahedral elements are used to represent the rigid RC beams, while 50 concrete finite elements (130 mm x 130 mm x 65 mm) and 318 steel embedded elements are used to discretize the RC domain.

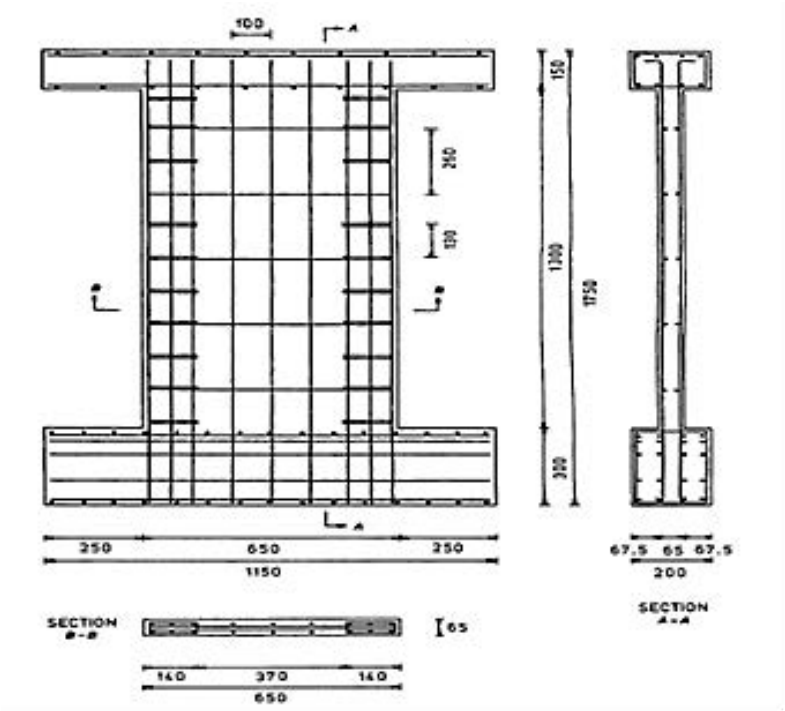

Figure 6 Geometric and reinforcement detail of the SW31 [17]

The numerical curves are compared with the corresponding experimental curve as can be depicted in Fig. 7. It is easy to observe that the numerical results are in good agreement with the experimental data in terms of stiffness and strength. The experimental results show that the specimens SW31 had a load-carrying capacity of 119 kN, respectively whereas the numerical predicted load-carrying capacity of the same specimens subjected to the same loading conditions is 121 kN. This is an error that is less than 2%.

The proposed model has used three approaches of smeared crack modelling for the needs of investigating the different available methods which are:

1. rotated (update crack plane for each iteration),
2. multidirectional (each crack can open in a different plane but remain fixed), and
3. fixed (cracks can open in certain crack planes and remain fixed) smeared crack model.

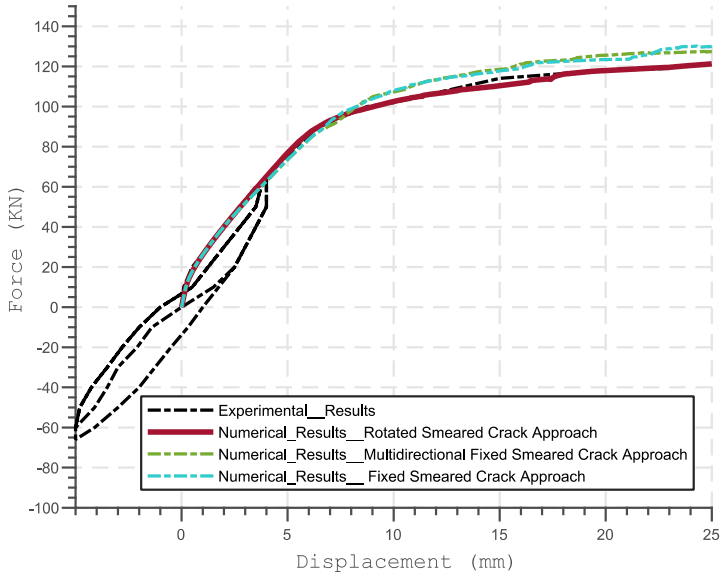

Figure 7 Comparison of the numerical results with the experimental data of the SW31.

The numerical results show that there is good agreement with the experimental data for all three crack approaches, thus similar responses are obtained. However, the model with the fixed approach (multidirectional and fixed smeared crack approach) derives a slightly stiffer behavior, especially in the post-cracking area.

The numerically obtained crack pattern of the RC shear wall specimen is illustrated in Fig. 8 when the maximum imposed displacement is reached. The cracks are formed within the areas of the section that are under tension due to the bending moment. Therefore, the cracks appear to be mainly horizontal. As the cracks form closer to the compressive zone of the section, they develop a relative inclination. Additionally, the figure shows a great concentration of cracks in the center of the shear wall which is dominated by a more complex state of stress due to triaxial phenomena attributed to the large normal and shear strains.

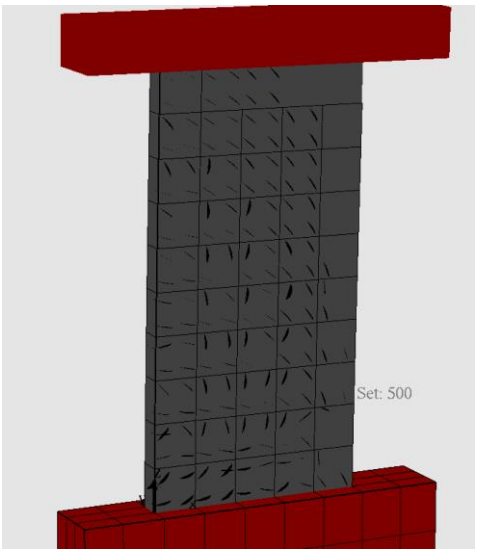

Figure 8 Crack pattern of the SW31 prior to failure.

6 CONCLUSIONS

This manuscript presents a conjunction of two constitutive modelling approaches for the simulation of concrete material in 3D. The modelling approach foresees that for the compressive behavior of the uncracked concrete, the material model proposed in [1] is used, whereas when the concrete is under tension, then it is modelled by using the constitutive material model as presented in [3]. The proposed material model which is a combination of a model derived from experimental data regression [1] and a model based on the thermodynamics law [3] was evaluated through the use of two experimental tests. According to the obtained numerical results, it was found that the combination of these two concrete material models produces a solid constitutive approach that can simulate accurately the nonlinear behavior of concrete when it develops extreme shear, which leads to a shear failure.

Future research work foresees the use of additional experimental data to be used for further validation of the proposed material model. In addition, the model will be expanded and integrated with the ability to capture the cyclic response of concrete. Further validation work will be performed in the case of cyclic loading conditions.

REFERENCES

[1] C. Mourlas, G. Markou, and M. Papadrakakis. "Accurate and computationally efficient non-linear static and dynamic analysis of reinforced concrete structures considering damage fac-tors". Engineering Structures, Vol. 178, pp. 258–285, Jan. 2019.

[2] Markou G, Garcia R, Mourlas Ch., Maurizio Guadagnini, Pilakoutas K., Papadrakakis M. "A New Damage Factor For Seismic Assessment Of Deficient Bare and FRP-Retrofitted RC Structures", Engineering Structures, Vol. 248,2021,113152.

[3] J. Červenka and V. K. Papanikolaou, "Three dimensionalcombined fracture–plastic material model for concrete,"International Journal of Plasticity, vol. 24, no. 12, pp. 2192–2220, 2008

[4] Kotsovos M.D. and Pavlovic M.N. (1995), Structural concrete. Finite Element Analysis for Limit StateDesign, Thomas Telford, London.

[5] Lykidis GC, Spiliopoulos K V. "An efficient numerical simulation of the cyclic loading experiments on RC structures". Computers and Concrete, Vol. 13(3), pp. 343–59, 2014.

[6] Moharrami M, Koutromanos I. "Finite element analysis of damage and failure of reinforced concrete members under earthquake loading". Earthquake Engineering & Structural Dynamics, Vol. 46(15), pp. 2811–29, 2017.

[7] Jason L, Huerta A, Pijaudier-Cabot G, Ghavamian S. "An elastic plastic damage formulation for concrete: Application to elementary tests and comparison with an isotropic damage model". Computer Methods in Applied Mechanics and Engineering, Vol. 195(52), pp. 7077–92, 2006.

[8] Richard B, Ragueneau F. "Continuum damage mechanics based model for quasi brittle materials subjected to cyclic loadings: Formulation, numerical implementation and applications". Engineering Fracture Mechanics, Vol. 98(1), pp. 383–406, 2013.

[9] G. Markou, C. Mourlas, H. Bark, and M. Papadrakakis. "Simplified HYMOD non-linear simulations of a full-scale multistory retrofitted RC structure that undergoes multiple cyclic excitations – An infill RC wall retrofitting study". Engineering Structures, Vol. 176, pp. 892–916, Dec. 2018.

[10] Markou G, Roeloffze W. Finite element modelling of plain and reinforced concrete specimens with the Kotsovos and Pavlovic material model, smeared crack approach and fine meshes. International Journal of Damage Mechanics. 2021;30(6):845-871. doi:10.1177/1056789520986601

[11] Bažant, Z.P., Oh, B.H., 1983. Crack band theory for fracture of concrete. Materials and Structures, RILEM 16 (3), 155–177.

[12] Willam K, Warnke EP. "Constitutive model for the triaxial behavior of concrete". Seminar on concrete structures subjected to triaxial stresses, Instituto Sperimentale Modeli e Strutture, Bergamo, Paper III-1., 1974.

[13] Hordijk, D.A., 1991. Local approach to fatigue of concrete. Ph.D. Thesis, Delft University of Technology, The Netherlands

[14] Rots, J.G., Blaauwendraad, J., 1989. Crack models for concrete: discrete or smeared? Fixed, multi-directional or rotating? Heron 34 (1)

[15] Leonhardt, F., Walther, R., 1962. Schubversuche an einfeldrigen stahlbetonbalken mit und ohne schubbewehrung. Deutscher Ausschuss fu¨r Stahlbeton, 151, Berlin, West Germany.

[16] Cervenka Consulting, ATENA software, https://www.cervenka.cz

[17] Lefas ID, Kotsovos MD. "Strength and Deformation Characteristics of Reinforced Concrete Walls Under Load Reversals". ACI Structural Journal, Vol. 87(6), pp. 716–26, 1990.